Petroleum Science 23 (2026) 236–244

Contents lists available at ScienceDirect

Petroleum Science

journal homepage: www.keaipublishing.com/en/journals/petroleum-science

Original Paper

Biomimetic inspired superhydrophobic nanofluids: Enhancing wellbore stability and reservoir protection in shale drilling

Jin-Sheng Sun [a,b,c], Ting Liao [b], Yu-Xi Ji [d], Hang Li [b], Yuan-Zhi Qu [c], Xian-Bin Huang [b], Kai-He Lv [b], Yu-Cai Luo [d], Bo Zhang [d], Jian Li [a,b,*]

[a] State Key Laboratory of Deep Oil and Gas, China University of Petroleum (East China), Qingdao, 266580, Shandong, China
[b] School of Petroleum Engineering, China University of Petroleum (East China), Qingdao, 266580, Shandong, China
[c] Drilling Fluid Research Institute, CNPC Engineering Technology R&D Company Limited, Beijing, 102206, China
[d] Huabei Oilfield Company, PetroChina Company Limited, Renqiu, 062552, Hebei, China

ARTICLE INFO

Article history:
Received 2 April 2025
Received in revised form
11 October 2025
Accepted 12 October 2025
Available online 15 October 2025

Edited by Jia-Jia Fei

Keywords:
Shale
Superhydrophobic nanofluids
Wetting inversion
Reduce self-priming
Inhibit hydration dispersion

ABSTRACT

Shale oil and gas, as typical unconventional resources, have gradually altered the global energy supply and demand landscape, attracting significant attention over recent decades. However, challenges such as wellbore instability and reservoir damage caused by drilling fluids invasion during shale drilling remain unresolved. In this study, we reported the synthesis and preparation of biomimetic inspired superhydrophobic nanofluids (SHN) with multiple functions by utilizing nano-silica, low surface energy fluorinated compounds, and cationic compounds with adsorption capabilities. Firstly, SHN with nano effects could plug micro-nano pores in shale, thereby reducing the filtration loss of drilling fluids (from 24 to 11 mL). Furthermore, SHN could adhere to shale surfaces through electrostatic interactions to increase its roughness from 1.121 to 3.567 μm, thereby transforming the shale surface from hydrophilic (26.4°) to superhydrophobic (152.8°). This not only reduced self-priming by 83.7% and decreased the capillary rise height to 5 mm below the liquid surface but also suppressed hydration expansion and improved the rolling recovery rate by 84.74%. Overall, this study provided new insights into the design and manufacturing of high-performance drilling fluids materials that could support wellbore stability and reservoir protection during shale oil and gas drilling processes.

1. Introduction

As global energy demand continues to rise, the rapid transformation of conventional oil and gas to unconventional oilfields has become inevitable (Fu and He, 2024). Shale oil and gas, characterized by abundant reserves and low-carbon energy sources, play a crucial role in the global energy system and economic development (Ma et al., 2018; Sun et al., 2021; Wei et al., 2021). Drilling serves as the primary way to establish a connection channel between shale formations and surface facilities (Li et al., 2021). Drilling fluids, commonly known as the “blood” of drilling engineering, serve essential functions such as suspending and transporting cuttings, balancing formation pressure, and supporting wellbore stability, which is crucial for the safe and efficient drilling of shale oil and gas.

However, shale oil and gas reservoirs are typically characterized by extremely low permeability, small matrix pore throats, and high clay mineral content (He et al., 2023). During the drilling process, the liquid phase of water-based drilling fluids tends to invade shale through fractures and pore throats, driven by both the action of pressure difference and capillary force (Abdullah et al., 2022; Gholami et al., 2018). The invasion of the water phase would weaken the mechanical properties of shale formation, increasing the risk of wellbore instability (Cheng et al., 2022). On the other hand, the water phase would cause hydration, expansion, and particle migration of shale clay, thus hindering the oil and gas permeation channels. What's more, the hydrophilic properties of the shale surface would cause water lock damage to shale pore throats, further exacerbating the damage to oil and gas reservoirs (Li et al., 2022; Zhao et al., 2021). Therefore,

* Corresponding author.
E-mail address: cuplijian@sina.com (J. Li).
Peer review under the responsibility of China University of Petroleum (Beijing).

https://doi.org/10.1016/j.petsci.2025.10.006

strengthening the wellbore stability and reservoir protection during shale oil and gas drilling presented critical challenges for water-based drilling fluids (Muhammed et al., 2021).

At present, nanotechnology has demonstrated broad application prospects in petroleum engineering, especially by using nanoparticles as additives to improve drilling fluids' performance (Mohammed et al., 2022). To address the challenges encountered by water-based drilling fluids for shale oil and gas, petroleum engineers have developed new nanomaterials for drilling fluids from the perspectives of physical plugging and chemical modification (Alkalbani and Chala 2024). Nano-plugging agents, including inorganic, organic, and inorganic-organic composite nanoparticles, could effectively plug nanoscale fractures in shale formations, reduce drilling fluids invasion, and prevent the transmission of formation pore pressure, thereby achieving wellbore stability and reducing reservoir damage (Li et al., 2023; Shen et al., 2022). In addition, changing the wettability of shale clay surface through chemical means could not only suppress the hydration expansion of shale but also reduce the water lock damage of drilling fluids, which would be beneficial for wellbore stability and reservoir protection (Jiang et al., 2022). For instance, Zhao et al. developed a novel complex binary system waterproofing locking agent, which exhibited excellent wettability reversal performance and significantly reduced capillary effects, effectively inhibiting the hydration swelling of shale clay (Zhao et al., 2022). Simultaneously, Wang et al. synthesized a polymer emulsion with multi-fluoromethyl structure, which significantly reduced surface energy and altered the wettability of the solid-liquid interface, effectively mitigating reservoir damage (Wang et al., 2021). In summary, although current plugging agents and wetting reversal agents have somewhat improved the interaction between liquids and shale surfaces, it still remains a great challenge to precisely design materials that could integrate multi-functions (plugging, wetting reversal, inhibition, etc.) into one structure.

Herein, inspired by the superhydrophobic mechanism triggered by the low interfacial energy substances and nano papillae on the surface of lotus leaves, a novel superhydrophobic nanofluids (SHN) with multiple functions including plugging, wetting alteration, and inhibition has been developed (Josyula et al., 2024; Wang et al., 2023). A series of experiments were conducted to assess SHN's ability to reduce drilling fluids filtration, change contact angle, decrease self-priming, and inhibit expansion. To further elucidate the mechanisms of SHN, methods such as SEM, 3D confocal microscopes, and nuclear magnetic resonance were also employed. Overall, SHN could enhance wellbore stability and reduce reservoir damage, providing new insights and technical support for safe and efficient drilling of shale oil and gas.

2. Materials and methods

2.1. Materials

Experimental reagents: nano-silica (30 nm, 99.5%), sodium dodecyl sulfate (99%), and potassium bromide (99.5%) were all sourced from Shanghai Huayuan Trading Century Co., Ltd. Dimethyl octadecyl(3-(trimethoxy silyl)propyl)ammonium chloride (DTSACI) was purchased from Wuhan Lanabai Pharmaceutical Chemical Co., Ltd. Additionally, triethoxy-1H,1H,2H,2H-tridecafluoro-*n*-octylsilane (PFOTES) was acquired from Shanghai Maier Biotechnology Co., Ltd. Ammonia water (25%) and anhydrous ethanol (99%) were sourced from China National Pharmaceutical Group Chemical Reagent Co., Ltd. Bentonite was sourced from Huai'an Bentonite Co., Ltd. The glass capillaries with an inner diameter of 0.5 mm were purchased from Qingdao Zhongshi Boyuan Biotechnology Co., Ltd. The shale samples were from outcrops in Sichuan Province, China, and the mineralogical composition of shale samples was presented in Table 1.

2.2. Preparation of superhydrophobic nanofluids (SHN)

18 g of silica nanoparticles were dispersed in a mixed solution consisting of 40 mL of anhydrous ethanol, 5 mL of ammonia water, 0.2 g of sodium dodecyl sulfate, and 60 mL of deionized water. The mixture was thoroughly stirred and ultrasonically dispersed for 20 min. The uniform suspension was poured into a four-necked flask equipped with a stirrer and a reflux condenser, and stirred in an oil bath at 70 °C for 30 min. Subsequently, 12 mL of DTSACI and 5 mL of PFOTES were added dropwise via a constant-pressure addition funnel. After refluxing for 24 h, the white emulsion product was obtained. The formulations containing solely DTSACI were labeled as E-SHN, those containing only PFOTES were designated as P-SHN, and those comprising both DTSACI and PFOTES were termed E/P-SHN. The synthesis schematic diagram of SHN was depicted in Fig. 1.

2.3. Characterization of superhydrophobic nanofluids (SHN)

Fourier infrared spectroscopy. A certain amount of SHN powder samples was blended with KBr and compressed into thin pellets using a compressor. The molecular structure and chemical functional group of SHN were characterized using a Nicolet iS20 FT-IR spectrometer.

X-ray photoelectron spectroscopy. The dried samples of SHN powder were compacted under a pressure of 50 MPa. The elemental composition of carbon (C), oxygen (O), silicon (Si), and fluorine (F) in the samples was characterized using a Kα electron spectrometer (Thermo Electron, USA).

Particle size distribution. Dilute the SHN sample to a suspension of 1 mg/mL and sonicate for 2 min to ensure uniform dispersion. Then the suspension was introduced into the sample cell, and the particle size distribution was measured at room temperature (25 °C) using the Malvern Zeta Sizer Nano ZS.

2.4. The performance of superhydrophobic nanofluids (SHN)

Rheology and filtration reduction. Different concentration of SHN was homogeneously dispersed in 4 wt% bentonite-based mud, stirred for 20 min, and then aged at 180 °C for 16 h. The apparent viscosity (AV), plastic viscosity (PV), and yield point (YP) of the drilling fluids were evaluated using a six-speed rotational viscometer. The API filtration was tested by using an SD medium-pressure filtration device, and the mud cakes from the API filtration experiments were subjected to a scanning electron microscope (SEM).

Contact angle measurement. Polished the shale core slices with 280 mesh sandpaper, and submerged them in SHN solutions of different concentrations for 24 h, followed by drying at constant weight. Then the water contact angle of the shale was measured using an optical contact angle instrument. Additionally, the

Table 1
Mineralogical composition of shale samples.

Composition	Content, wt%	Composition of clay mineral	Content, wt%
Quartz	35.9	Illite	50.4
Calcite	19.6	Kaolinite	11.7
Plagioclase	11.8	Illite/smectite mixed layer	37.9
Pyrite	3.0		
Clay mineral	29.7		

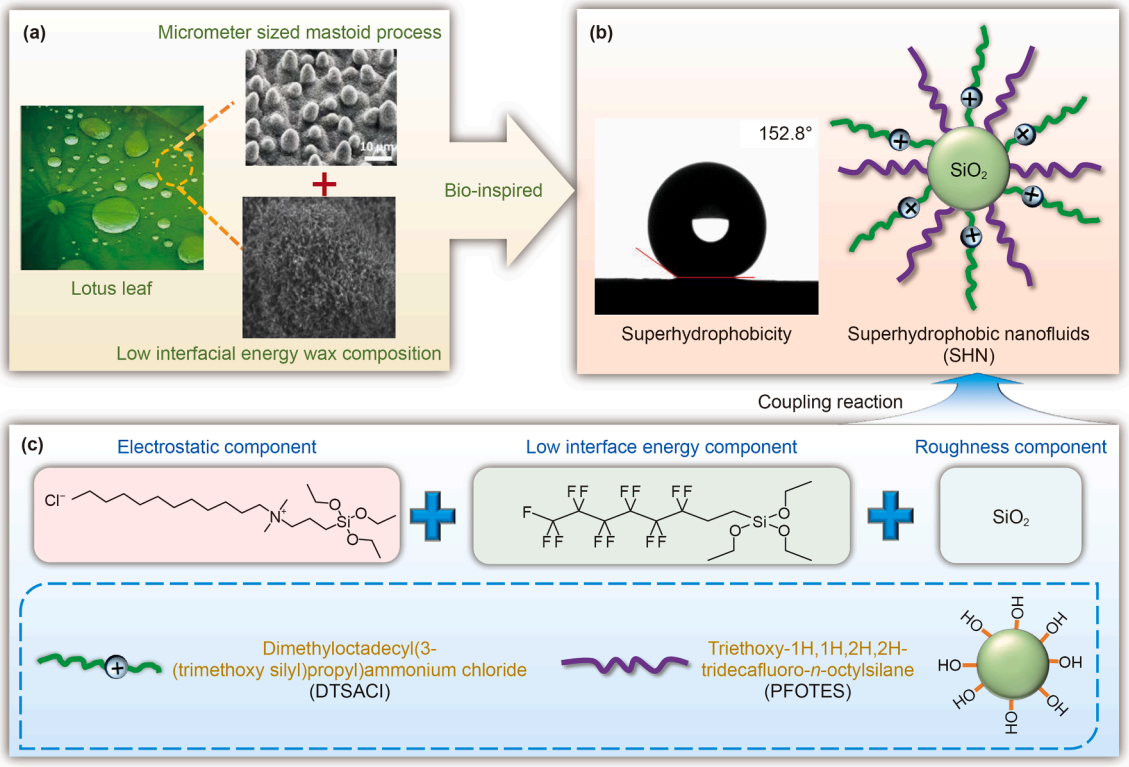

Fig. 1. Synthesis schematic diagram of superhydrophobic nanofluids (SHN).

microscopic morphology of shale was observed using both a scanning electron microscope (SEM) and a 3D confocal microscope.

Capillary rise experiment. The cleaned glass capillaries were immersed in SHN solutions of different concentrations for adsorption. After drying, the glass capillaries were vertically inserted into an evaporating dish filled with deionized water. The heights of the liquid levels under capillary action were observed and recorded.

Core natural imbibition. Before NMR T_2 spectrum measurements, the shale rock samples were vacuum-saturated with water for 24 h, followed by drying. These samples were then immersed in SHN solution and dried to a constant weight, placed in a beaker containing deionized water to a depth of 2–3 mm. After the reading stabilized, NMR T_2 spectrum measurements were conducted again.

Linear swelling test. Compress 10.05 g of dry shale powder sample through a core compactor and measure its original thickness. The swelling changes of the sample in the presence of various inhibitor solutions and SHN solutions were measured using a CPZ-II dual-channel linear dilatometer for 16 h.

Rolling recovery test. 50 g of shale cuttings were separately loaded into aging tanks containing SHN and different inhibitor solutions. After aging for 16 h, the hot-rolled shale cuttings were rinsed with water after being sieved through a 40-mesh size (0.42 mm), and the weight of the dried cuttings was recorded. Subsequently, the shale cuttings were crushed and washed three times with deionized water. The lower precipitate was dried and ground into powder at 80 °C, and X-ray diffraction (XRD) analysis was performed using a Rigaku Ultima IV instrument equipped with a Cu target. The percentage of shale recovery was calculated using the formula:

$$K = m/50 \times 100 \quad (1)$$

where K is the recovery rate of the shale cuttings (%); m is the weight of the shale cuttings after aging (g).

3. Results and discussion

3.1. Characterization of superhydrophobic nanofluids (SHN)

The grafting of DTSACI and PFOTES on the surface of nano silica particles was analyzed using Fourier transform infrared spectroscopy and elemental analysis. As illustrated in Fig. 2(a), the hydroxyl group vibration peak exhibited a notable red shift from 3441 to 3294 cm^{-1} along with reduced peak intensity, indicating that coupling reactions occurred between DTSACI, PFOTE compounds and the hydroxyl groups on the nano-silica surface (Pang et al., 2022; Qiao et al., 2022). The peaks at 2968 and 1435 cm^{-1} correspond to the stretching vibrations of $–CH_3$ and C–H groups, respectively. Specifically, the anti-stretching and bending vibrations peaks of the C–F bond at 1278 and 653 cm^{-1} further confirmed the successful grafting of PFOTES (Hozumi and Takai, 1996; Mousavi et al., 2013).

Fig. 2(b) displays the XPS survey spectra of the superhydrophobic nanofluids, with binding energies of 284.13, 532.08, 153.11, and 104.12 eV corresponding to C 1*s*, O 1*s*, Si 2*s*, and Si 2*p*, respectively. Notably, in the spectrum of P-SHN and E/P-SHN, a new peak at 685.2 eV was evident, corresponding to F 1*s*, indicating the successful modification with hydrophobic fluorine-containing segments on the silica surface (Ohno et al., 2023; Wei et al., 2020). Moreover, the high-resolution XPS spectra depicted in Fig. 2(c) demonstrated a new C–F binding energy peak at 284.4 eV in the C 1*s* XPS spectrum, further confirming the successful grafting of PFOTES (Cavallari et al., 2020; Chen et al., 2020). Therefore, based on the FT-IR and XPS analysis above, it could be verified that the cationic components (DTSACI) and low interfacial energy components (PFOTES) have been successfully grafted onto the surface of nano-silica particles.

Ulteriorly, as shown in Fig. 2(d) and (e), the nanofluids possessed a papillary spherical structure, with median particle sizes of 149.1,

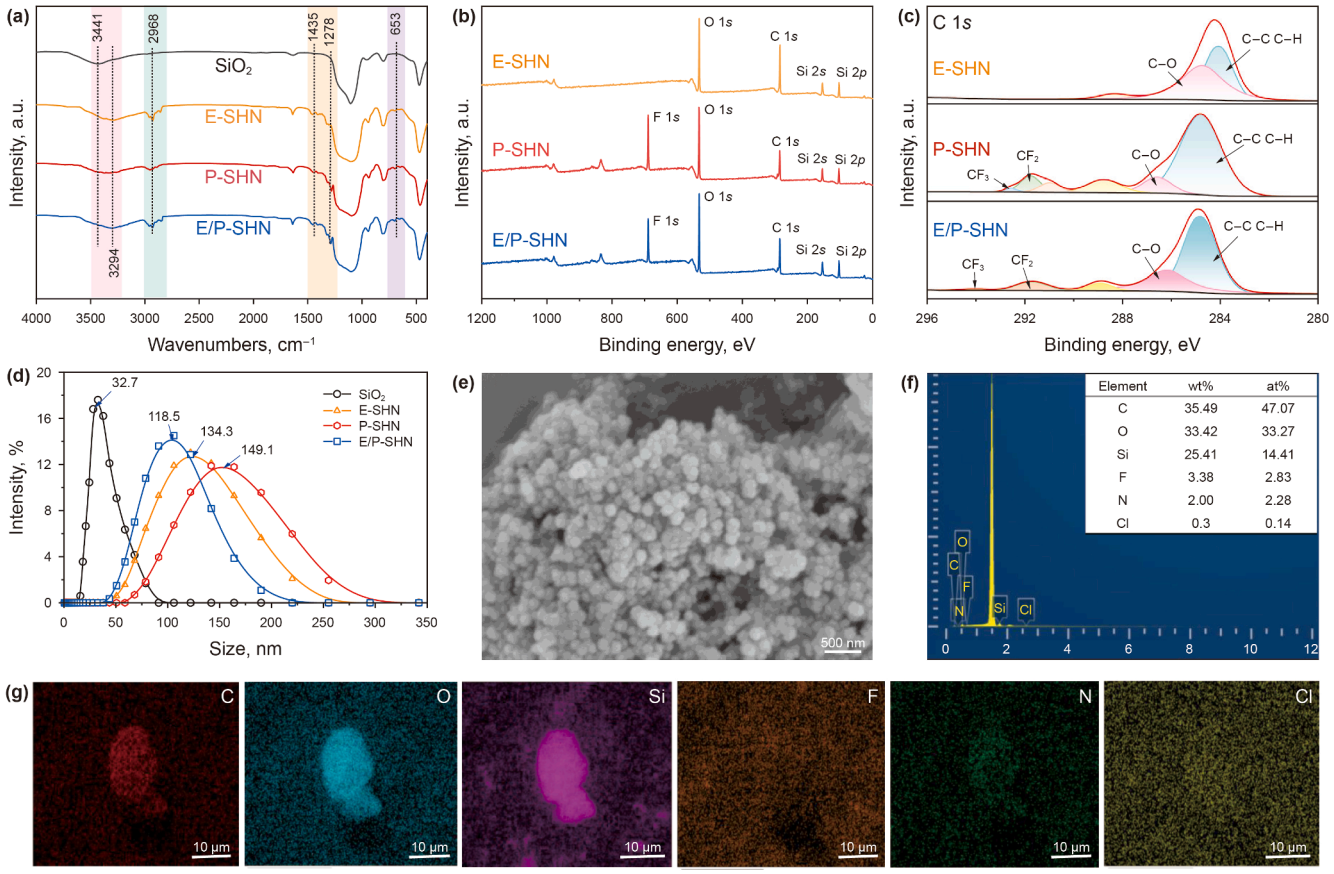

Fig. 2. **(a)** FTIR spectra of nano-silica and SHN; **(b)** Full XPS spectrum of the SHN; **(c)** C-spectrum analysis of SHN; **(d)** Particle size distribution of nano-silica and SHN; **(e)** SEM images of E/P-SHN; **(f)** EDS spectra of the E/P-SHN; **(g)** EDS mapping of C, O, Si, F, N, and Cl elements in E/P-SHN.

134.3, and 118.5 nm for E-SHN, P-SHN, and E/P-SHN, respectively. Notably, E/P-SHN demonstrated the smallest average particle size, an attribute that could be traced back to the strongly adsorbing cationic groups forming an electrical double layer on the nano-silica surface, enhancing interparticle electrostatic repulsion. Simultaneously, the hydrophobic fluorocarbon chains created steric hindrance due to the low surface energy, thereby reducing the tendency for particle agglomeration driven by surface energy (Fattahi et al., 2023; Hozumi and Takai, 1996). Consequently, the dispersibility of E/P-SHN in aqueous solutions surpassed that of both E-SHN and P-SHN, thus resulting in a relatively smaller particle size. In addition, the energy spectrum analysis in Fig. 2(f) and (g) demonstrated the presence of F, Cl, C, and N, further confirming that DTSACI and PFOTES were successfully modified on nano-silica particles during the reaction process.

3.2. Performance of SHN in drilling fluids

Additives are crucial for the rheological properties of drilling fluids, as they determine whether the drilling fluids can carry rock debris and fractured rocks (Lv et al., 2022). As shown in Fig. 3(a), the SHN solution exhibited shear dilution characteristics of non-Newtonian fluids, and the viscosity of E/P-SHN was lower than that of E-SHN and P-SHN at the same concentration. The impact of SHN on the rheological parameters and filtration properties of base slurry, both before and after aging, was evaluated according to API standards. The AV, PV, and YP of drilling fluids exhibited a positive correlation with the concentration of E/P-SHN. When 3 wt% E/P-SHN was added to the base slurry, the AV exhibited a significant increase from 5 to 14 mPa·s, the PV also rose from 4 to 10 mPa·s, while the YP increased from 1 to 4 Pa, and the FL_{API} decreased from 24 to 11 mL compared with pure base slurry. In addition, compared to E-SHN and P-SHN at the same concentration, E/P-SHN with smaller particle size had better adsorption properties, which promoted the dispersion of bentonite, resulting in lower viscosity increasing effect and better filtration reduction effect (Belayneh et al., 2021). Although the rheological parameters of drilling fluids decreased and the filtration loss increased to some extent after aging, which was because of the destruction of the network structure formed by bentonite in the high-temperature environment. Nevertheless, drilling fluids containing 3 wt% E/P-SHN still exhibited excellent rheological and filtration performance compared to the base slurry. The microstructure of the mud cake indicated that the surface of the mud cake formed by the base slurry contained microcracks, which provided a pathway for fluids invasion. In contrast, E/P-SHN could adsorb on the surface of bentonite and fill the microcrack pores of the mud cake, thereby reducing the filtration loss of drilling fluids.

3.3. Wetting reversal performance of superhydrophobic nanofluids (SHN)

Shale has high mineral content, developed nanopores and microcracks, strong hydrophilicity, and extremely strong self-priming ability for drilling fluids (Luo et al., 2022; Ma et al., 2021). As shown in Fig. 4(a) and (c), deionized water on the untreated shale surface rapidly diffused, with a water contact angle of 26.4°, exhibiting strong hydrophilic. In contrast, E/P-SHN enhanced its directional adsorption on shale surfaces through

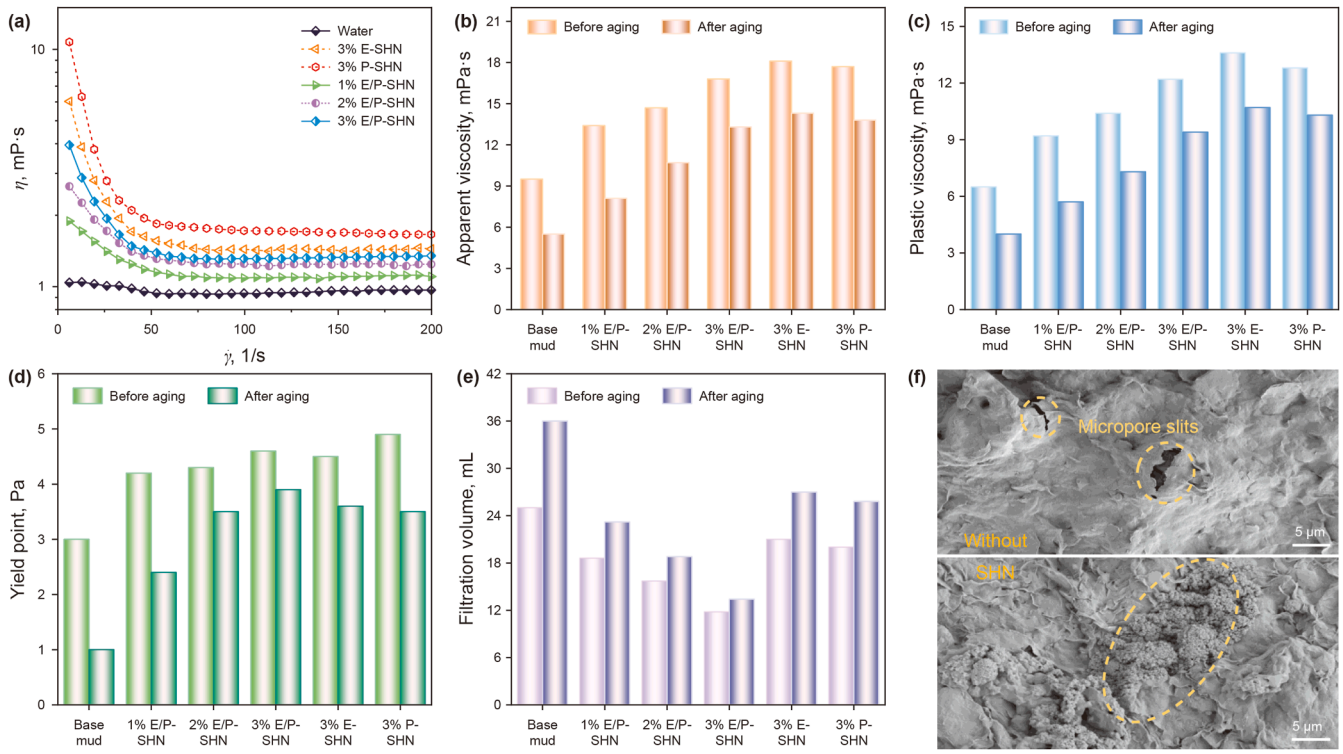

Fig. 3. **(a)** Viscosity curves of deionized water and SHN solutions; rheological and filtration properties of base slurry containing SHN: **(b)** AV; **(c)** PV; **(d)** YP; **(e)** filtration loss volume (FL_{API}); **(f)** microscopic morphology of mud cakes after aging of base slurry without and with SHN.

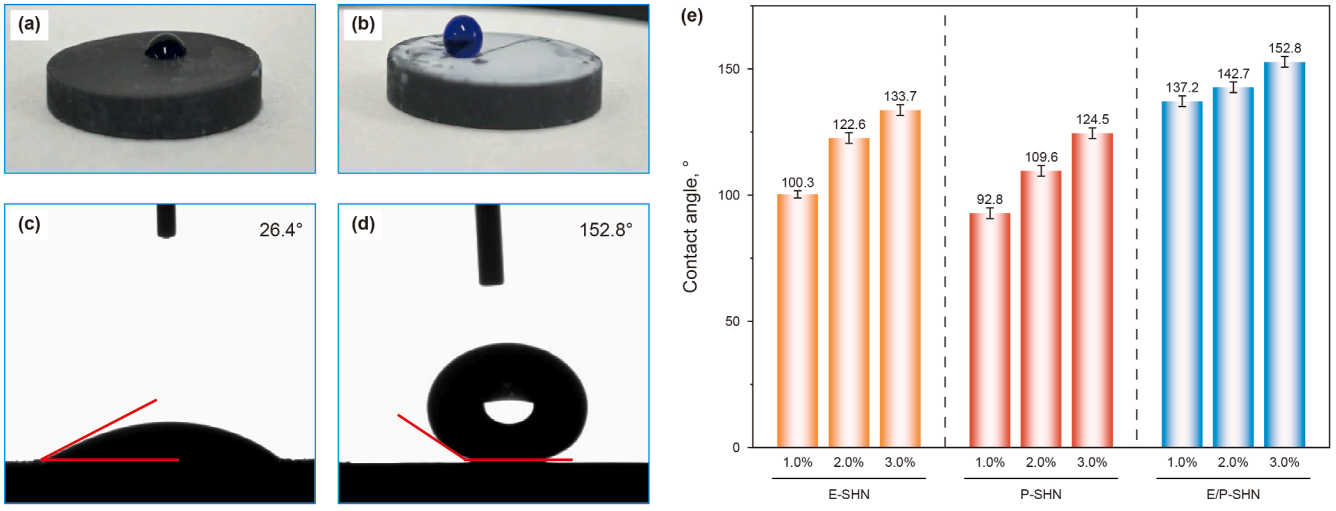

Fig. 4. **(a)** Wettability diagram of original shale; **(b)** wettability diagram of shale surface after treatment by E/P-SHN; **(c)** water contact angle diagram of original shale; **(d)** water contact angle diagram of shale surface after treatment by E/P-SHN; **(e)** contact angles of SHN at different concentrations.

electrostatic interactions between cationic component (DTSACl) and negative charges on the shale surface, and reduced the surface free energy of shale through the extremely low interfacial properties of fluorinated chains (PFOTES), thereby achieving superhydrophobicity on the shale surface. Thus, the shale surface supported stable spherical droplets, achieving a maximum water contact angle of 152.8°, illustrated in Fig. 4(b) and (d). The experimental results revealed a marked transformation in shale surface wettability from hydrophilic to superhydrophobic following treatment, effectively reducing the self-priming of drilling fluids. Moreover, comparative analysis in Fig. 4(e) demonstrated that the water contact angle on the shale surface treated with E/P-SHN was significantly higher than that for E-SHN and P-SHN treatments at the same concentration.

To further investigate the impact of superhydrophobic nanofluids on shale surface properties, the changes in micro-morphology and surface roughness of the shale before and after treatment were analyzed. Fig. 5(a) revealed that the untreated shale surface appeared relatively smooth in the SEM images, characterized by a layered structure composed of irregular rock particles and a surface roughness of 1.121 μm. After treatment with the superhydrophobic nanofluids, the SEM images revealed that the surface became rougher, as

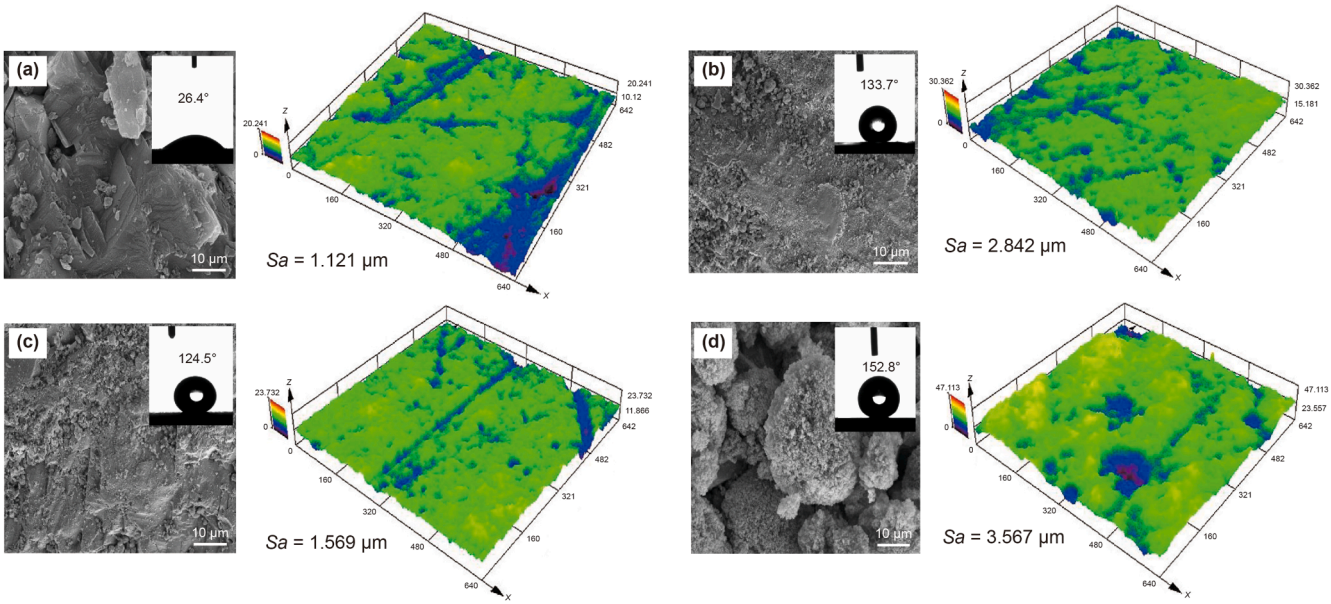

Fig. 5. SEM images and 3D morphology: **(a)** original shale; **(b)** after being treated by E-SHN; **(c)** after being treated by P-SHN; **(d)** after being treated by E/P-SHN.

numerous nanoparticles densely adhered and formed spherical particle aggregates of varying sizes, shown in Fig. 5(b)–(d). Specifically, the cationic component (DTSACl) endowed E-SHN and E/P-SHN with excellent adsorption capacity on shale surfaces, resulting in roughness of 2.842 and 3.567 μm, respectively. As a control, due to the absence of cationic components in P-SHN, its adsorption capacity on the shale surface was relatively weak, with a roughness of only 1.569 μm. Therefore, E/P-SHN not only contained cationic adsorption components that significantly improve roughness, but also hydrophobic fluorinated segments that endow low surface energy, thereby achieving the maximum contact angle on the shale surface compared to E-SHN and P-SHN.

3.4. Reducing self-priming performance of superhydrophobic nanofluids (SHN)

Under the action of capillary force, water in drilling fluids would spontaneously invade the pores and microcracks of shale, leading to wellbore instability and reservoir damage (Li et al., 2021; Zhang et al., 2023). The glass capillary ascent experiments, as well as the core self-absorption experiments, simulated the process of water entering the core under capillary force (Chen et al., 2025). As illustrated in Fig. 6(a) and (b), water ascended to a height of 49 mm in the untreated capillary, and the untreated core absorbed 3.01 g of water after 6 h of self-absorption, confirming that capillary force was the primary driving mechanism for water penetration. However, after treatment with SHN, the capillary force in the aqueous phase was reversed, and the rising height was reduced to below the liquid level. Specifically, the capillary tube treated with 3 wt% E/P-SHN had a liquid level height of −37 mm. Simultaneously, the self-priming adsorption capacity of the core also significantly decreased, with only 0.49 g in 3 wt% E/P-SHN solution. In addition, similar to the contact angle test results presented above, compared to E-SHN and P-SHN, E/P-SHN demonstrated superior performance in reducing water self-priming.

To further clarify the impact of superhydrophobic nanofluids on shale pore-throat imbibition, changes in the liquid-phase distribution of shale pore throats before and after treatment were analyzed. As shown in Fig. 5(c), the T_2 relaxation time distribution of water-saturated shale was wide (between 0.11 and 3.51 ms), with a high nuclear magnetic resonance signal intensity (over 1000), indicating that the pore throat structure was mainly composed of micropores, which could increase the self-priming effect of shale capillaries (Wen et al., 2024). By contrast, the NMR signal intensity of shale treated by E/P-SHN was significantly reduced, the pore throat volume was much smaller than that of water-saturated shale, and the relaxation time was somewhat extended. These changes proved that the superhydrophobic nanofluids effectively altered shale wettability and reduced capillary forces, leading to a significant decrease in water imbibition capacity, thereby preventing liquid-phase invasion.

3.5. Inhibition performance of superhydrophobic nanofluids (SHN)

Due to the abundant clay minerals in shale, linear expansion experiments were conducted to explore the inhibitory effects of superhydrophobic nanofluids (Zhang et al., 2024). As depicted in Fig. 7(a), the expansion rates of all samples initially increased and then stabilized. Specifically, the expansion rates of samples immersed in deionized water, 3% SiO_2, and 5% KCl for 16 h were 63%, 57%, and 48%, respectively. In comparison, the superhydrophobic nanofluids, particularly the E/P-SHN solution, significantly inhibited the linear expansion of samples, reducing it to just 17.6%. These results indicated that superhydrophobic nanofluids effectively suppress the linear expansion of samples, exhibiting superior inhibitory performance compared to ordinary inhibitors.

In addition, shale rolling recovery rate experiments simulated the fragmentation and dispersion of shale in high-temperature environments, further evaluating the inhibitory performance of superhydrophobic nanofluids. As shown in Fig. 7(b) and (d), the shale cuttings recovered from deionized water were scarce, with a rolling recovery rate of only 18.87%. At this time, the water molecules intensified surface hydration and permeation hydration of the shale cuttings. However, in the E/P-SHN solution, the rolling recovery rate increased significantly to 84.74%, and the recovered cuttings exhibited a large and numerous phenomena. Notably, the recovery rate in the E/P-SHN solution was superior to that in the KCl and SiO_2 solutions.

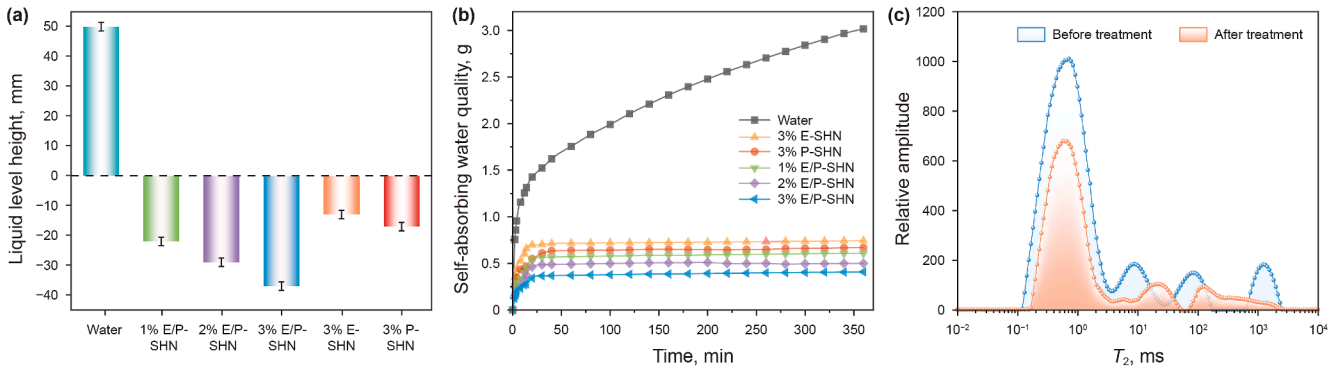

Fig. 6. **(a)** Capillary self-absorption height before and after treatment by SHN; **(b)** water imbibition volume of shale before and after E/P-SHN treatment; **(c)** NMR T_2 spectrum of shale before and after E/P-SHN treatment.

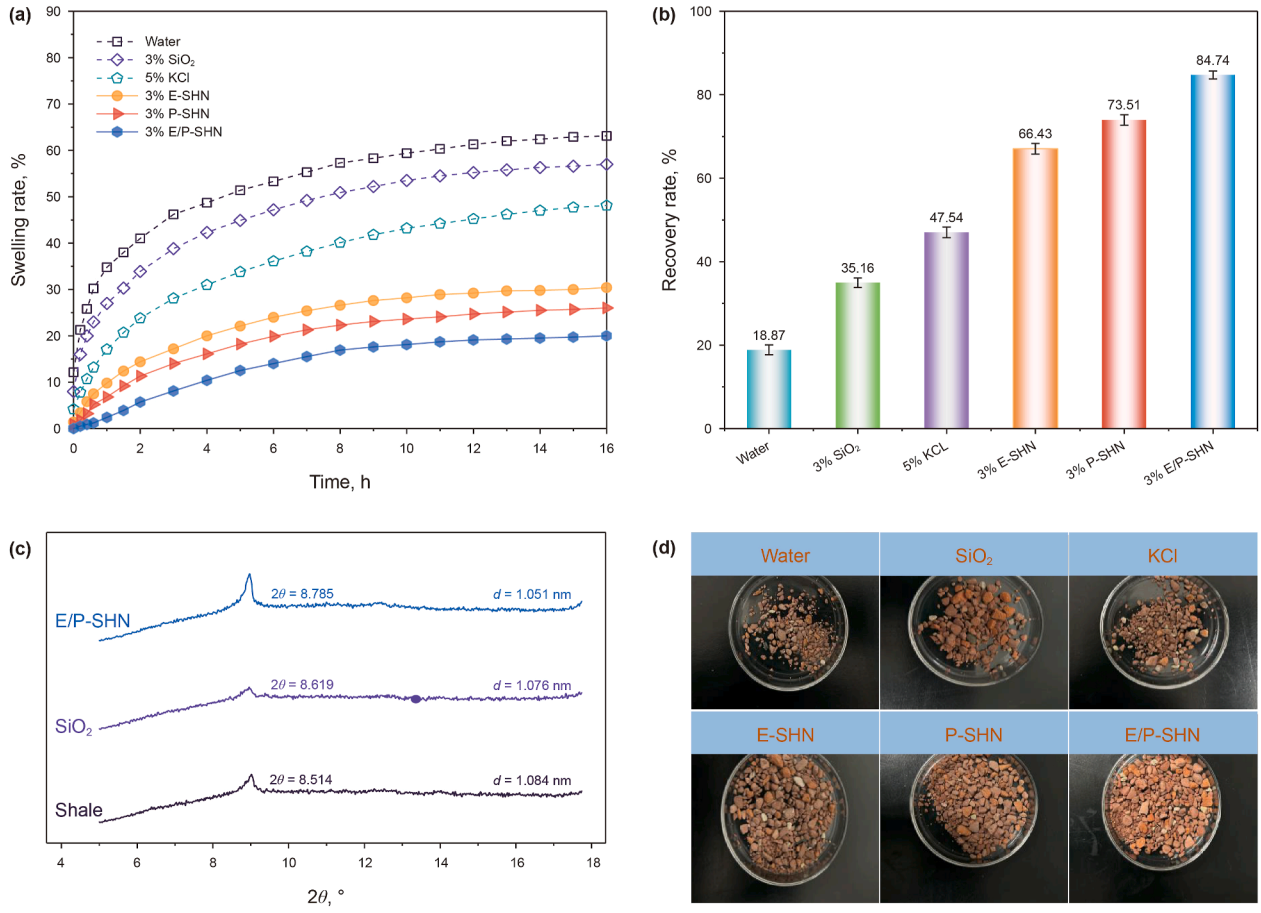

Fig. 7. **(a)** Linear swelling ratios of the sample in different inhibitors and SHN; **(b)** recovery rates of shale in different inhibitors and SHN; **(c)** X-ray diffraction (XRD) patterns of shale cuttings after rolling recovery; **(d)** image of shale cuttings after rolling recovery.

To further elucidate the effect of superhydrophobic nanofluids on shale inhibitory hydration and dispersion, X-ray diffraction (XRD) analysis was performed on the shale cuttings used in the experiment. Fig. 7(c) illustrated that the interlayer spacing slightly decreased after adding 3% E/P-SHN. Compared with the interlayer spacing of shale, the particle size of E/P-SHN was larger and unable to embed into the interlayer of clay to suppress osmotic hydration. Based on the micromorphology of shale and contact angle results, it could be concluded that E/P-SHN achieves the transformation of shale surface from hydrophilic to superhydrophobic through electrostatic adsorption, thereby preventing water from entering the interlayer and inhibiting surface hydration. Therefore, E/P-SHN could improve the rolling recovery rate of shale and enhance the wellbore stability during drilling.

3.6. *Mechanism of superhydrophobic nanofluids (SHN)*

The control mechanism of wellbore stability and reservoir protection during the drilling process in shale oil and gas, facilitated by superhydrophobic nanofluids, was shown in Fig. 8 based on the experimental results above. Usually, shale has a high mineral content, developed nanopores and microcracks, and exhibits

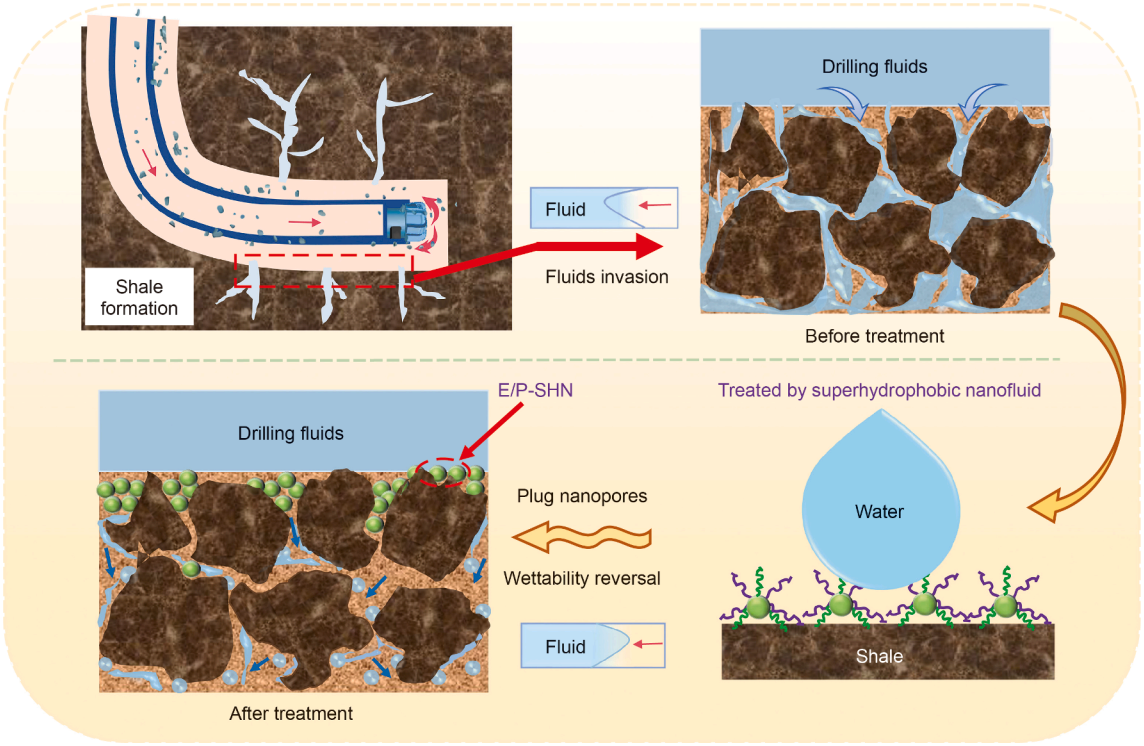

Fig. 8. Schematic diagram of the mechanism of E/P-SHN enhancing shale wellbore stability and reservoir protection.

strong hydrophilicity. As a result, drilling fluids are prone to invade the reservoir under pressure differences and capillary force, leading to wellbore instability and reservoir damage during the drilling process (Shi et al., 2018). Superhydrophobic nanofluids, with nanoscale effects, could be filled in the nanoscale pores and fractures of shale to form a plugging layer, thereby reducing the invasion of drilling fluids. Additionally, E/P-SHN could be adsorbed onto the shale surface via electrostatic interactions, increasing the surface roughness and reducing its surface energy, thereby transforming the shale surface from hydrophilic to superhydrophobic. This not only prevented water molecules from interacting with the shale, inhibiting the hydration expansion of shale, but also significantly reduced the self-priming of drilling fluids, further strengthening the wellbore stability and reservoir protection during shale drilling.

4. Conclusions

In this study, inspired by the superhydrophobicity of lotus leaves, a novel superhydrophobic nanofluid (SHN) with multiple functions was developed by modifying nano-silica with low surface energy fluorinated compounds and cationic long-chain alkanes with adsorption capacity. The fundamental physicochemical properties of SHN were analyzed by FT-IR, XPS, and SEM. Furthermore, the comprehensive performance of SHN, such as reducing the filtration loss, altering the wettability of the shale surface, reducing the self-priming, and inhibiting shale hydration expansion, was evaluated. Based on the results, the following specific conclusions were drawn:

(1) Drilling fluids containing 3 wt% E/P-SHN exhibited a reduction in filtration loss from 24 to 11 mL, compared to the base slurry, demonstrating the excellent filtration reduction performance of E/P-SHN.
(2) E/P-SHN significantly altered the wettability of shale, increasing the contact angle from 26.4° to 152.8°, causing the shale surface to transition from hydrophilic to superhydrophobic.
(3) E/P-SHN converted capillary force into liquid phase invasion resistance, thereby significantly reducing the self-absorption water content of shale rock.
(4) E/P-SHN efficiently adsorbed onto the surface of shale and inhibited its surface hydration, significantly improving the rolling recovery rate of shale.

In summary, superhydrophobic nanofluids are essential in reducing filtration loss, reversing wettability, reducing self-priming, and inhibiting hydration, providing effective solutions for wellbore stability and reservoir protection during shale oil and gas drilling.

CRediT authorship contribution statement

Jin-Sheng Sun: Supervision. **Ting Liao**: Writing-review & editing, Writing-original draft, Conceptualization. **Yu-Xi Ji**: Data curation. **Hang Li:** Writing-original draft. **Yuan-Zhi Qu:** Funding acquisition. **Xian-Bin Huang:** Conceptualization. **Kai-He Lv:** Supervision, Conceptualization. **Yu-Cai Luo:** Conceptualization. **Bo Zhang:** Supervision. **Jian Li:** Writing-review & editing, Writing-original draft, Funding acquisition.

Declaration of competing interest

In this article, during the research design, data analysis, and paper writing processes, we declare that there were no financial conflicts of interest. Additionally, no personal relationships that could affect the research work were involved.

Acknowledgments

The authors are thankful to the National Natural Science Foundation of China (Nos. 52204023 and 52474022), the Key R&D Program of Shandong Province (2024CXPT076), Mount Taishan Scholar Program of Shandong Province (tsqn202408111) and China Petroleum Science and Technology Innovation Fund (2023DQ02-0304).

References

Abdullah, A.H., Ridha, S., Mohshim, D.F., et al., 2022. A comprehensive review of nanoparticles: effect on water-based drilling fluids and wellbore stability. Chemosphere 308, 136274. https://doi.org/10.1016/j.chemosphere.2022.136274.

Alkalbani, A.M., Chala, G.T., 2024. A comprehensive review of nanotechnology applications in oil and gas well drilling operations. Energies 14 (7), 798. https://doi.org/10.3390/en17040798.

Belayneh, M., Aadnøy, B., Strømø, S.M., 2021. Mos_2 nanoparticle effects on 80 °C thermally stable water-based drilling fluid. Materials 14 (23), 7195. https://doi.org/10.3390/ma14237195.

Cavallari, C., Radescu, S., Dubois, M., et al., 2020. Tuning c–f bonding of graphite fluoride by applying high pressure: experimental and theoretical study. J. Phys. Chem. C 124 (45), 24747–24755. https://doi.org/10.1021/acs.jpcc.0c06860.

Chen, C., Zhuo, S., Li, S., et al., 2025. Wettability modification of a nano-silica/fluoro surfactant composite system for reducing the damage of water blocking in tight sandstone reservoirs. RSC Adv. 15 (7), 5264–5276. https://doi.org/10.1039/d4ra08564g.

Chen, X., Wang, X., Fang, D., 2020. A review on c1s xps-spectra for some kinds of carbon materials. Fullerenes, Nanotub. Carbon Nanostruct. 28 (12), 1048–1058. https://doi.org/10.1080/1536383x.2020.1794851.

Cheng, R., Lei, Z., Bai, Y., et al., 2022. Preparation of the tetrameric poly(vs-st-bma-ba) nano-plugging agent and its plugging mechanism in water-based drilling fluids. ACS Omega 7 (32), 28304–28312. https://doi.org/10.1021/acsomega.2c02784.

Fattahi, R., Lashkarbolooki, M., Abedini, R., et al., 2023. Investigating the synergistic/antagonistic effects of mixing sio_2 nanoparticles and ionic liquid, nonionic emulsifier, and gemini surfactants on the main mechanisms of crude oil production. Energ Fuel 37 (19), 14741–14751. https://doi.org/10.1021/acs.energyfuels.3c02569.

Fu, E., He, W., 2024. The development and utilization of shale oil and gas resources in China and economic analysis of energy security under the background of global energy crisis. J. Pet. Explor. Prod. Technol. 14, 2315–2341. https://doi.org/10.1007/s13202-024-01818-3.

Gholami, R., Elochukwu, H., Fakhari, N., et al., 2018. A review on borehole instability in active shale formations: interactions, mechanisms and inhibitors. Earth Sci. Rev. 177, 2–13. https://doi.org/10.1016/j.earscirev.2017.11.002.

He, Y., Jiang, G., Dong, T., et al., 2023. Research progress and development tendency of polymer drilling fluid technology for unconventional gas drilling. Front. Energy Res. 10, 1058412. https://doi.org/10.3389/fenrg.2022.1058412.

Hozumi, A., Takai, O., 1996. Effect of hydrolysis groups in fluoro-alkyl silanes on water repellency of transparent two-layer hard-coatings. Appl. Surf. Sci. 103 (4), 431–441. https://doi.org/10.1016/s0169-4332(96)00534-x.

Jiang, G., Sun, J., He, Y., et al., 2022. Novel water-based drilling and completion fluid technology to improve wellbore quality during drilling and protect unconventional reservoirs. Engineering 18, 129–142.

Josyula, T., Kumar, M.L., Thomas, T.M., et al., 2024. Fundamentals and applications of surface wetting. Langmuir 40 (16), 8293–8326. https://doi.org/10.1021/acs.langmuir.3c03339.

Li, H., Sun, J., Lv, K., et al., 2021. Wettability alteration to maintain wellbore stability of shale formation using hydrophobic nanoparticles. Colloid. Surface. A 635, 128015. https://doi.org/10.1016/j.colsurfa.2021.128015.

Li, J., Fan, J., Deng, X., et al., 2023. Functionalized nano core-shell polystyrene spheres with polyionic liquids: an efficient shale stabilizer with both inhibit hydration and physical plugging. Geoenergy Sci. Eng. 236, 212571. https://doi.org/10.1016/j.geoen.2023.212571.

Li, J., Sun, J., Lv, K., et al., 2022. Temperature- and salt-resistant micro-crosslinked polyampholyte gel as fluid-loss additive for water-based drilling fluids. Gels 8 (5), 289. https://doi.org/10.3390/gels8050289.

Luo, X., Jiang, G., Wang, G., et al., 2022. Novel approach to improve shale stability using super-amphiphobic nanoscale materials in water-based drilling fluids and its field application. Rev. Adv. Mater. Sci. 61 (1), 41–54. https://doi.org/10.1515/rams-2022-0003.

Lv, K., Du, H., Sun, J., et al., 2022. A thermal-responsive zwitterionic polymer gel as a filtrate reducer for water-based drilling fluids. Gels 8 (12), 832. https://doi.org/10.3390/gels8120832.

Ma, J., Xia, B., An, Y., 2021. Advanced developments in low-toxic and environmentally friendly shale inhibitor: a review. J. Petrol. Sci. Eng. 208, 109578. https://doi.org/10.1016/j.petrol.2021.109578.

Ma, Y., Cai, X., Zhao, P., 2018. China's shale gas exploration and development: understanding and practice. Petrol. Explor. Dev. 45 (4), 589–603. https://doi.org/10.1016/s1876-3804(18)30065-x.

Mohammed, A., Shadfar, D., David, A., et al., 2022. Nanoparticle applications as beneficial oil and gas drilling fluid additives: a review. J. Mol. Liq. 352, 118725. https://doi.org/10.1016/j.molliq.2022.118725.

Mousavi, M.A., Hassanajili, S., Rahimpour, M.R., 2013. Synthesis of fluorinated nano-silica and its application in wettability alteration near-wellbore region in gas condensate reservoirs. Appl. Surf. Sci. 273, 205–214. https://doi.org/10.1016/j.apsusc.2013.02.014.

Muhammed, N.S., Olayiwola, T., Elkatatny, S., 2021. A review on clay chemistry, characterization and shale inhibitors for water-based drilling fluids. J. Petrol. Sci. Eng. 206, 109043. https://doi.org/10.1016/j.petrol.2021.109043.

Ohno, R., Shudo, K., Tano, T., et al., 2023. Development of polymer composite membranes with hydrophilic tio2 nanoparticles and perfluorosulfonic acid-based electrolyte for polymer electrolyte fuel cells operating over a wide temperature range. Acs. Appl.Energ. Mater 6 (19), 10098–10104. https://doi.org/10.1021/acsaem.3c01721.

Pang, Y., Zhao, C., Li, Y., et al., 2022. Cadmium adsorption performance and mechanism from aqueous solution using red mud modified with amorphous mno2. Sci. Rep-Uk 2022 (14), 4424. https://doi.org/10.1038/s41598-022-08451-2.

Qiao, S., Yu, H., Wang, Y., et al., 2022. Foam stability of temperature-resistant hydrophobic silica particles in porous media. Front. Chem. 2022 (10), 960067. https://doi.org/10.3389/fchem.2022.960067.

Shen, Y., Zhu, Y., Gao, Z., et al., 2022. Nano-sio_2 grafted with temperature-sensitive polymer as plugging agent for water-based drilling fluids. Arabian J. Sci. Eng. 48, 9401–9411. https://doi.org/10.1007/s13369-022-07486-x.

Shi, Y., Chen, S., Yang, X., et al., 2018. Enhancing wellbore stability of coal measure strata by electrical inhibition and wettability control. J. Petrol. Sci. Eng. 174, 544–552. https://doi.org/10.1016/j.petrol.2018.11.052.

Sun, C., Nie, H., Dang, W., et al., 2021. Shale gas exploration and development in China: current status, geological challenges, and future directions. Energ Fuel 35 (8), 6359–6379. https://doi.org/10.1021/acs.energyfuels.0c04131.

Wang, X., Hassan, A., Boudaoud, H., et al., 2023. A review on 3d printing of bio-inspired hydrophobic materials: oil-water separation, water harvesting, and diverse applications. Adv. Compos. Hybrid Mater. 6, 170. https://doi.org/10.1007/s42114-023-00740-2.

Wang, Y., Liang, L., Li, Y., et al., 2021. Preparation and application of a fluoropolymer emulsion as novel wettability reversal agent. Colloid. Surface. A. 612, 125985. https://doi.org/10.1016/j.colsurfa.2020.125985.

Wei, J., Duan, H., Yan, Q., 2021. Shale gas: will it become a new type of clean energy in China? — a perspective of development potential. J. Clean. Prod. 294, 126257. https://doi.org/10.1016/j.jclepro.2021.126257.

Wei, J., Li, B., Jing, L., et al., 2020. Efficient protection of mg alloy enabled by combination of a conventional anti-corrosion coating and a superamphiphobic coating. Chem. Eng. J. 390, 124562. https://doi.org/10.1016/j.cej.2020.124562.

Wen, X., Chen, Y., Pu, R., 2024. Analysis of the factors influencing movable fluid in shale oil reservoirs: a case study of chang 7 in the ordos basin, China. Geomech. Geophys. Geol. 10, 177. https://doi.org/10.1007/s40948-024-00899-y.

Zhang, F., Wang, Y., Wang, B., et al., 2024. Organosiloxane-modified auricularia polysaccharide (Si-ap): improved high-temperature resistance and lubrication performance in wbdfs. Molecules 29 (11), 2689. https://doi.org/10.3390/molecules29112689.

Zhang, K., Liu, X., Wang, D., et al., 2023. A review of reservoir damage during hydraulic fracturing of deep and ultra-deep reservoirs. Pet. Sci. 21 (1), 384–409. https://doi.org/10.1016/j.petsci.2023.11.017.

Zhao, P., Fan, X., Zhang, Q., et al., 2021. Characteristics of hydration damage and its influence on permeability of lamellar shale oil reservoirs in ordos basin. Geofluids (1), 15. https://doi.org/10.1155/2021/6646311.

Zhao, X., Liu, M., Ma, C., et al., 2022. Performance evaluation of an octadecyltrimethyl ammonium chloride–dimethyl silicone oil as a waterproof locking agent in low-permeability reservoirs. ACS Omega 7 (36), 31954–31960. https://doi.org/10.1021/acsomega.2c02878.